EPJ Web of Conferences **112**, 01004 (2016)
DOI: 10.1051/epjconf/201611201004

Deeply Virtual Compton Scattering on the Neutron: JLab Experiment E08-025

Meriem BENALI[1,2,3,a], Malek MAZOUZ[2,3], Helene FONVIEILLE[1]

[1] *Laboratoire de Physique Corpusculaire Clermont-Ferrand, IN2P3, 63177 Aubière Cedex, France*
[2] *Faculté des Sciences de Monastir, 5000, Tunisia*
[3] *For the Hall A DVCS collaboration*

Abstract.
This paper gives the preliminary results of the experimental cross section for deeply virtual Compton scattering on the neutron ($en \rightarrow en\gamma$). The E08-025 experiment was performed at Jefferson Lab Hall A. We measured the $(D(e, eX - H(e, e'\gamma)X)$ unpolarized cross section and we extracted, for the first time, a non-zero contribution of (neutron-DVCS + coherent-deuteron-DVCS) at $Q^2 = 1.75\ GeV^2$ and $x_B = 0.36$.

1 Introduction

The electromagnetic probe is a very important tool to investigate the properties of the nucleon. This technique has been used to measure the nucleon form factors by elastic scattering [1] and the partons distribution functions through inclusive deep inelastic scattering [2]. While elastic scattering allowed access to spatial distributions of charge and current in the nucleon, the deep inelastic scattering provides information about parton's longitudinal momentum and helicity distributions in the nucleon. Unfortunately, these two separate informations do not allow multi-dimensional description of the nucleon, any spatial information remains inaccessible in inclusive DIS. In the mid-90's, a new theoretical framework has been developed, namely the generalized parton distributions (GPDs) [3–5] , which relates the elastic form factors and the ordinary parton distributions. In addition, these observables give information about the angular momentum of partons which is an important element to solve the "spin crisis" problem [4, 6]. Indeed, the longitudinal projection of the nucleon spin (= 1/2) is written according to Jaffe an Manohar's decomposition as [7]:

$$1/2 = \frac{\Delta\Sigma}{2} + \Delta G + L_q + L_g$$

where $\Delta\Sigma$ is the intrinsic spin contribution of quarks which is measured ($\Delta\Sigma \approx 0.34$) [8, 9], ΔG is the gluons spin contribution and is also determined [9, 10] and L_q, L_g are respectively the orbital momentum of quarks and gluons wich are unknown so far. However, Ji [4] demonstrated that the GPDs give access to the quarks (and gluons) angular momentum contribution to the nucleon's spin (Ji's sum rule):

[a] e-mail: benali@jlab.org

$$J_q = \frac{1}{2}\Delta\Sigma_q + L_q = \frac{1}{2}\int_{-1}^{+1} xdx[H_q(x,\xi,t=0) + E_q(x,\xi,t=0)].$$

At leading order, the GPDs are four universal functions $H_q(x,\xi,t)$, $E_q(x,\xi,t)$, $\tilde{H}_q(x,\xi,t)$ and $\tilde{E}_q(x,\xi,t)$ defined for each quark flavor q. They depend on the momentum fraction (x), the DVCS scaling variable(ξ) and the momentum transfer (t). The GPDs can be accessed by the hard exclusive processes. The simplest one is the "Deeply Virtual Compton Scattering". At the Bjorken limit, defined by a large virtuality $Q^2 \to \infty$, high energy of the virtual photon $\nu \to \infty$ and fixed Bjorken variable $x_B = \frac{Q^2}{2M\nu}$, where M is the nucleon mass, this process can be factorized into two parts: a known perturbative part ($\gamma^* q \to \gamma q$) and non-perturbative part which is parametrized by GPDs as shown in Figure 1.

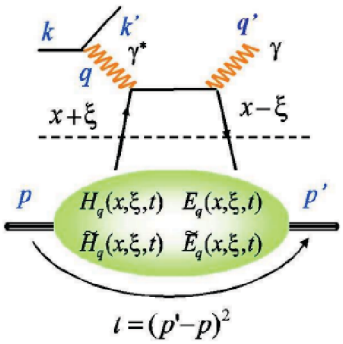

Figure 1. Handbag diagram for the DVCS process.

Motivated by the importance of these observables, different DVCS experiments were performed. The first Beam spin asymmetries were measured by HERMES [11] and CLAS [12]. The H1 [13] and ZEUS [14] collaborations measured the DVCS cross section at low x_B. The first measurements of DVCS cross section in the valence quark region were performed at JLAB Hall A [15]. The first extraction of DVCS on the neutron and the first experimental constraint on the GPD E was obtained at JLab Hall A [16]. DVCS beam-spin asymmetries and target spin asymetries were determined in JLab Hall B using CLAS [17, 18]. The E08-025 experiment was performed at JLab Hall A in 2010 in order to measure the n-DVCS cross section, which is sensitive to the GPD E (the less constrained GPD). The data were taken at fixed $Q^2 = 1.75\ GeV^2$ and $x_B = 0.36$ but at two beam energies $E_{beam} = 4.45\ GeV$ and $E_{beam} = 5.54\ GeV$. In this experiment, 15 cm liquid deuterium (D_2) and hydrogen (H_2) targets are used. The photon electroproduction on a deuterium target can be decomposed into: coherent $d(e,e'\gamma)d$ and incoherent $p(e,e'\gamma)p$ and $n(e,e'\gamma)n$ contributions:

$$D(e,e'\gamma)X = p(e,e'\gamma)p + n(e,e'\gamma)n + d(e,e'\gamma)d + ...$$

As shown in figure 2, each contribution is the sum of the DVCS process and the Bethe-Heitler (BH) process where the real photon is emitted by the incoming or the scattered electron.

The BH amplitude is fully calculable using the form factors so measuring the experimental cross section of the $n(e,e'\gamma)n$ process leads to the determination of the $|DVCS|^2$ plus the interference term. Finally, two measurements at fixed x_B and Q^2 but at two different beam energies allow the separation of the $|DVCS|^2$ and the interference terms.

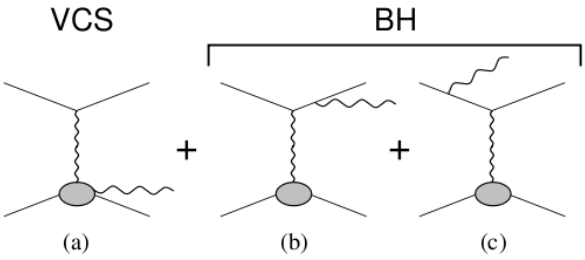

Figure 2. (a): The DVCS process, (b) and (c) Bethe-Heitler process diagrams

The DVCS on the neutron is deduced by comparing the data taken on hydrogen and deuterium targets. The scattered electron is detected in a High Resolution Spectrometer (Left-HRS) in coincidence with the DVCS photon detected in an electromagnetic calorimeter. The recoil nucleon is identified with the missing mass technique. The electromagnetic calorimeter is a matrix of 13×16 PbF_2 blocks, placed at $1.1m$ from the target, centered around the virtual photon direction which leads to a momentum transfer t ranging roughly from -0.1 to -0.5 GeV^2. Each block is connected to (PM + electronic base + ARS) which are equivalent to a numeric oscilloscope recording signals on $128ns$. The main goal of using ARS is to deal with pile up signals in our high luminosity experiment. Due to radiation damage the optical properties of the PbF2-blocks deteriorate during the experiment leading to an overall decline of blocks gain. For this reason, the first step in our analysis is the calorimeter energy calibration.

2 Calorimeter energy calibration

Two elastic calibrations, based on $ep \rightarrow e'p'$ elastic reaction, are performed during our experiment but cannot provide a daily calibration [20]. So we performed a second calibration where we used $H(e,e'\pi^0)X$ and $D(e,e'\pi^0)X$ data which have been taken simultaneously with DVCS data. The calibration method is based on the comparison between the measured energy of a detected π^0 (using the energy deposit in calorimeter) and its expected energy calculated with its scattering angle (also given by the calorimeter) [19]. The invariant mass of $\gamma\gamma$ events detected in the calorimeter provides a good test of this calibration. Figure 3 shows the invariant mass peak position versus data group number. After the calibration, the points representing the new invariant mass peak position are aligned with the exact π^0 mass. To check our calibration, we compared the missing mass squared peak position (of the same data), corresponding to $H(e,e'\pi^0)p$ exclusive events, before and after this calibration for each group of data. After the calibration we reproduce, as shown in Figure 4, the nucleon mass squared ($0.88\ GeV^2$) for each group number.

Thanks to this π^0 calibration method and to the daily switching between hydrogen and deuterium targets during data taking, we obtained a daily calibration of the calorimeter energy. This allows to reduce the systematic error on the results coming from the energy calibration of the calorimeter.

3 Selection of exclusive photon electroproduction events

The DVCS events are selected with a cut on the missing mass squared $M_X^2 = (k + p - k' - q')^2 < (M + M_{\pi^0})^2 \approx 1.15\ GeV^2$. Below this cut, we have only $H(e,e'\gamma)p$ (or $D(e,e'\gamma)pn$) events (called DVCS events), but these events are contaminated by:

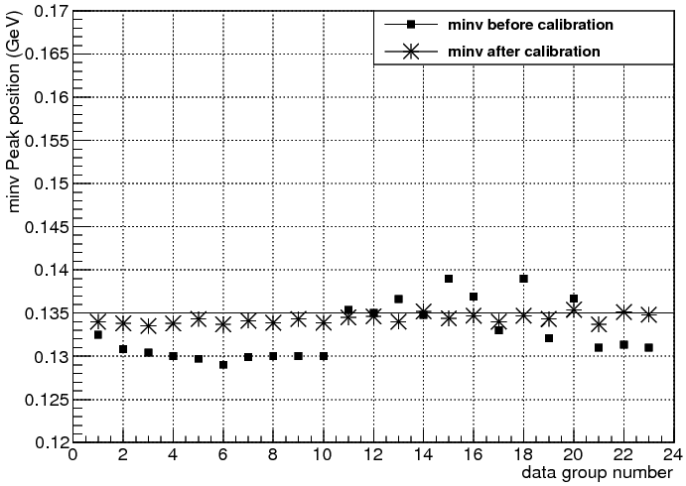

Figure 3. Invariant mass peak position as a function of data group number before and after π^0 calibration. The solid horizontal line represents the π^0 mass.

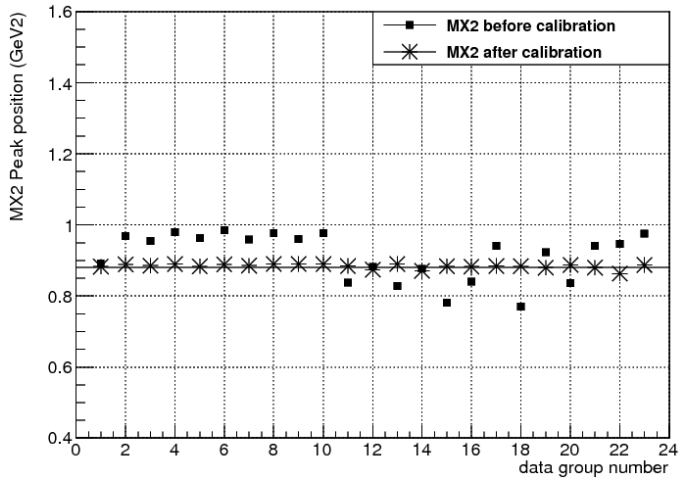

Figure 4. Missing mass squared peak position as a function of data group number before and after π^0 calibration. The solid horizontal line represents the nucleon mass squared.

- Accidental coincidences : when the detected photon in the calorimeter is in fortuitous coincidence with the scattered electron.
- π^0 contamination : when the detected photon in the calorimeter comes from the asymmetric decay of π^0, this photon resembles kinematically to a DVCS photon. We substract the π^0 contamination by using a clean sample of detected π^0 from $H(e,e'\pi^0)X$ or $D(e,e'\pi^0)X$. For these events, a simulation of all possible $\pi^0 \to \gamma\gamma$ decays tells us which fraction of asymmetric decays is seen as DVCS events [20].

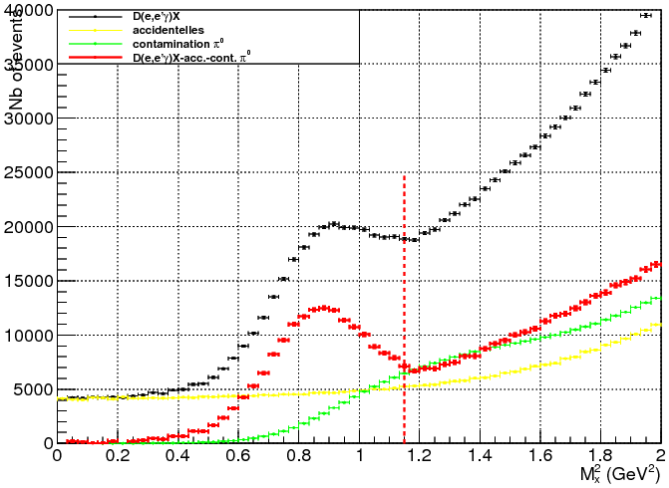

Figure 5. Missing mass squared spectrum of raw data (black), accidental data (yellow), π^0 contamination (green), and after all substractions (blue spectrum) for $D(e,e'\gamma)X$, "Kin2 low" kinematics.

Figure 5 shows the spectrum of the missing mass squared M_X^2 for $D(e,e'\gamma)X$ raw data, the accidental coincidences and the π^0 contamination events for one kinematic (called Kin2Low: $E_{Beam} = 4.45GeV$). Before subtracting the $H(e,e'\gamma)p$ events from $D(e,e'\gamma)pn$) events, we added Fermi momentum [21] to H2 data and normalized H2 and D2 data to the same luminosity. The $D(e,e'\gamma)X - H(e,e'\gamma)X$ data are represented by the purple spectrum in figure 6. This spectrum contains the DVCS on the neutron events (n-DVCS) and also the DVCS on the coherent-deuteron events (d-DVCS). The vertical line represents the missing mass squared cut at the pion production threshold. These experimental data are used to extract the (n-DVCS + d-DVCS) cross section.

4 Smearing of the simulation data

The extraction of the cross section is done using the experimental data and the simulation data. First, it is necessary to have a good matching between the experimental data and simulated data (having the same exclusive peak position and having the same resolution). Our method is based on smearing the photon energy for each event in the simulation, because the experimental resolution is dominated by the energy resolution of the calorimeter. Since the extraction of the cross section is performed by bins in t and in ϕ (the angle between the hadronic and leptonic planes), our smearing method was applied for each of these bins independently. Figure 7 shows a spectrum of the missing mass squared of the $H(e,e'\gamma)p$ data (blue) and the proton simulated data after smearing (red), a good agreement between the two spectra is clear below the pion production threshold.

5 Extraction of the cross section

The experimental data ($D(e,e'\gamma)X - H(e,e'\gamma)X$) contain a neutron contribution (n-DVCS) and a coherent deuteron contribution (d-DVCS). In this case, the unpolarized photon electroproduction cross section can be written as [22]:

$$\frac{d^4\sigma}{dQ^2 dx_B dt d\phi} = \sigma(BH_n) + \sigma(BH_d) + \sum_{in}(\Gamma_{in}(Q^2, x_B, t, \phi)X_{in}) + \sum_{id}(\Gamma_{id}(Q^2, x_B, t, \phi)X_{id}), \qquad (1)$$

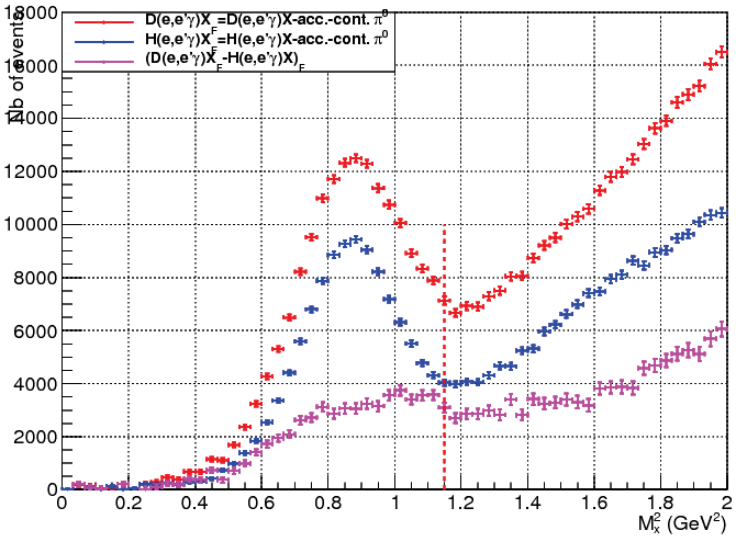

Figure 6. Missing mass squared spectrum of ($D(e,eX$- accidental - π^0contamination) events (red), ($H(e,e'\gamma)X$- accidental - π^0 contamination) events (blue) and ($D(e,e'\gamma)X - H(e,e'\gamma)X$). The purple spectrum represents the (n-DVCS+deuteron-coherent-DVCS) events at the left of the vertical line which is the pion production threshold.

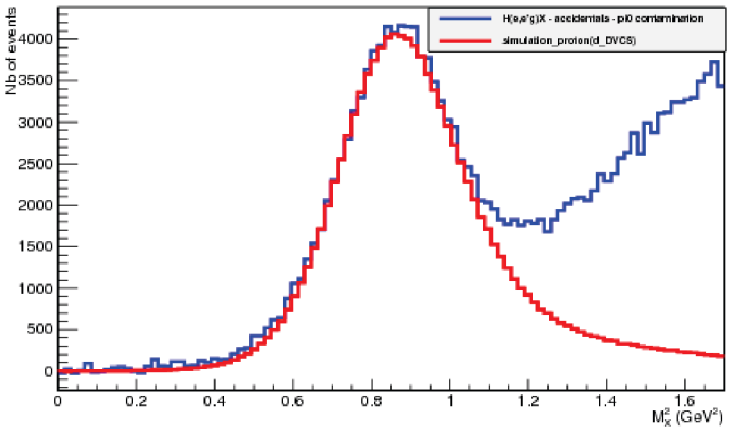

Figure 7. Missing mass squared spectrum of the $H(e,e'\gamma)p$ data (blue specrum) and the proton simulation data (red spectrum).

where the indices (n/d) signify respectively (neutron/deuteron-coherent), BH is the Bethe-Heitler contribution and $\Gamma_i(Q^2, x_B, t, \phi)$ is a calculable kinematical factor which depends on the kinematics variables. (X_{in}, X_{id}) are the unknown harmonics that we want to extract; these observables are linear combinations of Compton Form Factors (CFFs) which contain the GPDs observables. The depen-

dence on ϕ in the kinematical factors allows us to separate the contribution of the different harmonics (for the neutron or the coherent-deuteron) and a binning in M_X^2 is important to separate the contributions of the neutron from the ones of coherent-deuteron.

In order to extract the observables X_{in} and X_{id} given by equation 1, we performed a χ^2 minimization between the experimental number of events, N^{exp}, and the simulated number of events, N^{sim}.

$$\chi^2 = \sum_{k=1}^{Nbin} \left(\frac{N_k^{sim} - N_k^{exp}}{\Delta N_k^{exp}}\right)^2. \tag{2}$$

Note the summation over all bins at the vertex k (5 bins in t × 20 bins in ϕ= 100 bins). ΔN_k^{exp} is the experimental statistical error in one bin k.

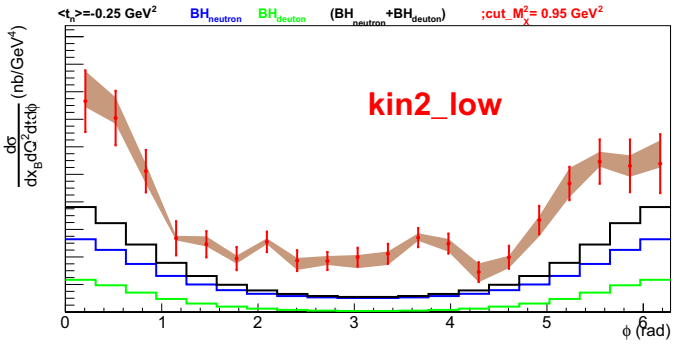

Figure 8. Preliminary results of $(n(e,e'\gamma)n + d(e,e'\gamma)d)$ experimental cross section (black points), neutron BH contribution (blue histogram), coherent-deuteron BH contribution (green histogram) and BH-sum (black histogram) for one bin at $< t >= -0.25\ GeV^2$ and the kinematic Kin2Low. Error bars are statistical and the shaded area is the systematic error.

Figure 8 shows the preliminary results of the experimental cross section corresponding to the sum $(n(e,e'\gamma)n + d(e,e'\gamma)d)$, for one bin at $< t >= 0.25\ GeV^2$ for one kinematic Kin2Low. These results show for the first time the existence of a positive contribution of n-DVCS (+ d-DVCS) which is observed at both beam energies. These results are obtained after testing their stability as a function of the upper M_X^2 cut.

5.1 Conclusion

In summary, our analysis of this experiment provides preliminary results of the experimental cross section $(n(e,e'\gamma)n + d(e,e'\gamma)d)$. For the first time, we have found a positive contribution of n-DVCS (+ d-DVCS) at both beam energies. We plan to make more stability and correlation studies to estimate separately the contributions n-DVCS and d-DVCS and a global fit will be performed using data at both energies to extract CFFs.

References

[1] V. Punjabi et al., Eur.Phys.J. A51, 79 (2015) and references therein.
[2] H. Abramowicz et al, Eur.Phys.J. C75 (2015) 12, 580 and references therein.

[3] D. Muller et al., Fortschr. Phys. 42, 2101 (1994).
[4] X. Ji, Phys. Rev. Lett. 78, 610 (1997).
[5] A.V. Radyushkin, Phys. Lett. B 380, 417 (1996).
[6] J. Ashman t al, Nucl. Phys. B 328, 1 (1989).
[7] R.L. Jaffe and A. Manohar, Nucl. Phys. B 337 (1990) 509.
[8] D. Hash, Nucl. Phys. B (Proc. Suppl.) 191 (2009) 79-87.
[9] V.Y. Alexakhin et al., Phys. Lett. B 647 (2007) 8.
[10] E.S. Ageev et al., Phys. Lett. B 633 (2006) 25.
[11] A. Airapetian et al. (HERMES), Phys. Rev. Lett. 87, 182001 (2001).
[12] S. Stepanyan et al. (CLAS), Phys. Rev. Lett. 87, 182002(2001).
[13] C. Adloff et al. (H1), Phys. Lett. B 517, 47 (2001).
[14] S. Chekanov et al. (ZEUS), Phys. Lett. B573, 46 (2003).
[15] C. Munoz Camacho et al., Phys. Rev. Lett. 97, 262002 (2006).
[16] M. Mazouz et al. Phys.Rev.Lett. 99, 242501 (2007).
[17] F.X Girod et al. Phys.Rev.Lett. 100, 162002 (2008).
[18] S. Pisano et al. Phys.Rev. D91, 052014 (2015).
[19] M. Mazouz, DVCS internal note, (2011).
[20] C. Munoz Camacho, PhD thesis, Université Paris VI,(2005).
[21] M. Garcon and J.W. Van Orden. Adv. Nucl. Phys. 26, 293 (2001).
[22] A.V. Belitsky et al, Phys.Rev. D82, 074010 (2010).